Optics & Laser Technology 169 (2024) 110097

Contents lists available at ScienceDirect

Optics and Laser Technology

journal homepage: www.elsevier.com/locate/optlastec

Full length article

Investigation of Laser-Induced Surface Structures (LIPSS) on quartz and evaluation of their influence on material wettability

Raffaele De Palo [a,b], Antonio Emanuele Mazzarone [a,c], Annalisa Volpe [a,b,*], Caterina Gaudiuso [b], Francesco Paolo Mezzapesa [b], Vincenzo Spagnolo [a,d], Antonio Ancona [a,b]

[a] Dipartimento Interateneo di Fisica, Politecnico di Bari & Università degli Studi di Bari, Via G. Amendola 173, Bari 70125, Italy
[b] National Research Council of Italy, IFN CNR, Institute for Photonics and Nanotechnologies, Via Amendola 173, Bari 70125, Italy
[c] Dipartimento di Fisica, Università di Pavia, Via A. Bassi 6, Pavia 27100, Italy
[d] PolySense Innovations srl, Via Amendola 173, Bari 70126, Italy

ARTICLE INFO

Keywords:
LIPSS
Femto-second laser
Wettability
Quartz crystal

ABSTRACT

We report here on a study of the generation of Laser-Induced Periodic Surface Structures (LIPSS) on quartz upon irradiation with linearly polarized femto-second laser pulses (pulse duration $\tau = 200$ fs and central wavelength $\lambda = 1030$ nm). Two different regimes of LIPSS were observed, Low-Spatial-Frequency-LIPSS (LSFL) and High-Spatial-Frequency-LIPSS (HSFL), characterized by different spatial periods and orientations. The formation of these two types of structures was investigated by varying the laser fluence, the number of laser pulses and the laser repetition rate. Once established how these parameters affect the generation of LIPSS, extended HSFL patterns (25×25 mm^2) were realized, and their wettability was compared to that of pristine quartz. Contact angle measurements showed that HSFL textured quartz exhibits a super-hydrophilic behaviour, with a measured contact angle equal to 7.6°, with respect to pristine quartz which results simply hydrophilic and shows a contact angle equal to 41.2°.

1. Introduction

Silicon dioxide, commonly known as quartz, is the most abundant mineral on earth. Its most relevant properties are chemical stability and piezoelectricity [1]; these two characteristics make quartz an excellent material for sensing technology devices such as Quartz-Tuning-Forks (QTF) [2] or Quartz-Crystal-Microbalance (QCM) [3]. QTFs transducers are employed in Quartz-Enhanced-Photoacoustic-Spectroscopy (QEPAS) [4] or Light-Induced-Thermoelastic-Spectroscopy (LITES) [5,6], while QCMs are used typically as electrochemical sensors [7]. These applications could greatly benefit from the surface functionalization of quartz in order to tailor the properties of the employed quartz-based devices. One of the most advanced and reliable techniques for texturing and functionalization of solid surfaces is Ultra-Short-Pulsed-Laser (USPL) processing. This method has been consistently used for changing the optical [8], electrical [9] and mechanical [10–13] properties of materials. The leading edge of USPL surface functionalization is represented by texturing the surfaces with Laser-Induced-Periodic-Surface-Structures (LIPSS). LIPSS are highly ordered and periodic structures which most often manifest themselves in the form of ripples whenever the target material is irradiated by linearly polarized sub-nanosecond laser pulses with fluence close to the material damage threshold [14]. Their orientation is dependent on the laser beam polarization direction. Two distinct types of LIPSS are usually observed: Low-Spatial-Frequency LIPSS (LSFL) and High-Spatial-Frequency LIPSS (HSFL). LSFL present spatial periods $\lambda/2 < \Lambda_{LSFL} < \lambda$ and their orientation is perpendicular to laser beam polarization for most materials [15,16], with some exceptions for very large band gap dielectrics, where they were found parallel to the beam polarization [17]. HSFL spatial periods are smaller than half the irradiation wavelength ($\Lambda_{HSFL} < \lambda/2$) and have been observed predominantly on transparent materials, with orientation typically perpendicular [17,18] and sometimes parallel to the polarization [19]. Most works investigating LIPSS applications are focused on metals (such as gold, aluminium, steel, platinum, titanium, etc.) and semiconductors for structural colour generation [20], alteration of wetting properties [21], tribology [22] and support for cellular growth on textured surfaces [14,23]. One relevant application on a dielectric material is the enhancement of optical absorption of diamond

* Corresponding author.
E-mail address: annalisa.volpe@poliba.it (A. Volpe).

https://doi.org/10.1016/j.optlastec.2023.110097
Received 10 July 2023; Received in revised form 18 August 2023; Accepted 15 September 2023
Available online 18 September 2023

with LIPSS texturing [9,24]. LIPSS formation has been investigated for quartz [17], but to our knowledge, there are no studies in literature regarding possible applications of quartz surfaces functionalized with LIPSS.

In this work, we evaluate how experimental parameters such as laser fluence F, number of laser pulses N and repetition rate ν affect the generation of LIPSS on quartz surfaces. The possibility of producing LIPSS patterns over extended areas (up to 25 mm^2) was also investigated. Such extended patterns were then verified to have an impact on the material wettability, making LIPSS-textured quartz a superhydrophilic material and a reliable alternative for humidity sensing applications [25].

2. Materials and experimental setup

Double polished z-cut quartz wafers, produced by Nano Quartz Wafer GmbH, were employed. The wafers had an area of 25.4 x25.4 mm^2, with a thickness of 400 ± 50 μm and a surface roughness Ra of 3 nm.

The texturing apparatus employed in this work is schematically represented in Fig. 1.

A Pharos SP 1.5 from Light Conversion was employed as laser system. It radiates an almost diffraction limited beam ($M^2 = 1.3$, certified by the producing company) characterized by pulses with tunable duration from 190 fs to 10 ps, with a central wavelength at 1030 nm, a maximum pulse energy E_P of 1.5 mJ and a maximum average power of 6 W. The pulse repetition rate ν is tunable from single pulse to 1 MHz. In our setup, the linearly polarized beam passed through a half-wave plate and a polarizer; the coupling of these two optics allowed the rotation of the laser polarization and the fine tuning of the laser power. The linear polarizer transmitted the P component of polarization. The pulse duration was set at 200 fs. The laser beam was directed to a PC-controlled galvo scanner (SCANLAB intelliSCAN$_{SE}$ 14) equipped with a 100 mm-F-theta lens. The upper surface of the quartz sample was placed on the focal plane of the F-theta lens. The estimated beam waist w in air was 12.5 μm.

The influence of the laser irradiation conditions on the LIPSS morphology was investigated by producing a series of round spots and varying the following laser parameters, i.e., laser fluence F, repetition rate ν, number of pulses N and laser polarization direction.

Extended LIPSS patterns were then realized based on the results from the single spot experiments. Such patterns were dependent also by the scanning speed V of the laser beam and the hatch distance h between scanning tracks, following two irradiation schemes as sketched in Fig. 2.

For such patterns, the laser fluence was set at $F = 5$ J/cm^2 and the number of pulses per spot at $N = 10$, calculated as $N_{pps} = d\,\nu/V$, where d is the beam diameter, ν the laser repetition rate and V is the scanning speed. In both patterns the scanning speed was perpendicular to the polarization direction. This value of F was chosen since it is slightly lower than the laser ablation threshold at $N_{pps} = 10$ [26]. Being d equal to 25 μm, ν was set at 0.6 kHz and V = 1.5 mm/s. These patterns extended over a square area of 25 mm^2.

The characterization of each textured sample was performed using two microscopes: an optical microscope (Nikon Eclipse E600) and a Scanning-Electron-Microscope (Zeiss Mod Sigma). Before SEM imaging all samples were sonicated in ethanol and then metallized through evaporation of gold. This last process is required because SEM imaging of dielectrics materials is difficult and affected by poor resolution. The SEM acquired LIPSS images that were subsequently processed by means of the Fourier transform (FT) using the Gwyddion software, to determine the spatial period of the laser-induced structures. The wetting behaviour of the LIPSS-textured patterns was investigated by performing contact angle measurements using a digital goniometer. Such device consisted of a Dino-lite portable microscope and a cold light lamp for backlighting the droplet. 3 μL droplets were deposited on the patterns by means of a micropipette (GILSON Pipetman). The superficial resistivity of the LIPSS patterns were directly measured using a digital multimeter after having exposed such patterned samples in a vapour chamber, consisting of a transparent plastic box with one entrance for the vapour generator (ARCOMA Biemmedue) and another one for a humidity sensor (RS PRO) probe.

3. Results and discussion

3.1. LIPSS period dependence on laser fluence

At first, the variation of LIPSS type and period as a function of the laser fluence F was evaluated. Once set the number of pulses and the repetition rate, respectively, at $N = 10$ and $\nu = 6$ KHz, F was increased from 5 to 10 J/cm^2. These parameters were chosen, from a previous work [26], since they were expected to be close enough to the ablation threshold, which is a prerequisite for obtaining LIPSS. In Fig. 3, SEM images of five spots realized at increasing F values are shown.

At the lowest fluence values $F = 5$ J/cm^2 and 5.5 J/cm^2, HSFL were observed, with orientation perpendicular to the laser beam polarization. At $F = 6.5$ J/cm^2, LSFL can be observed in the center of the irradiated spot and parallel to laser beam polarization (POL B). For higher fluences (8.5 J/cm^2 and 10 J/cm^2), LSFL become more extended and regular, especially at the fluence of 10 J/cm^2. Another series of spots was realized with the same working parameters of Fig. 2 but rotating the polarization of 90° (POL A). Again, the HSFLs arranged themselves perpendicular to the polarization direction and the LSFLs were found parallel to the polarization. In Fig. 4 LIPSS periods are reported as function of the laser fluences for both series of spots realized with orthogonal polarizations.

Fig. 4 clearly shows that around $F = 6$ J/cm^2 there is a transition

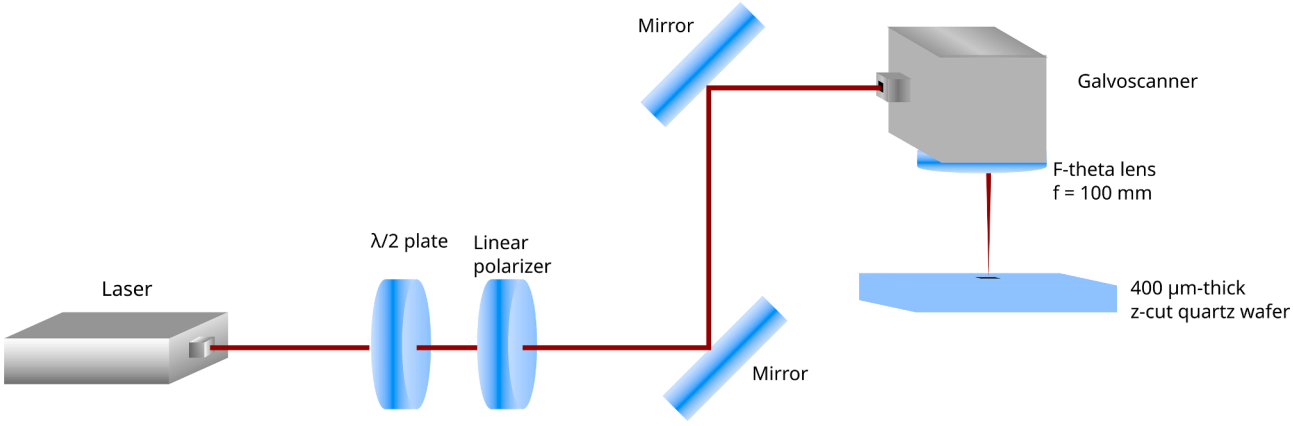

Fig. 1. Schematic design of the texturing setup.

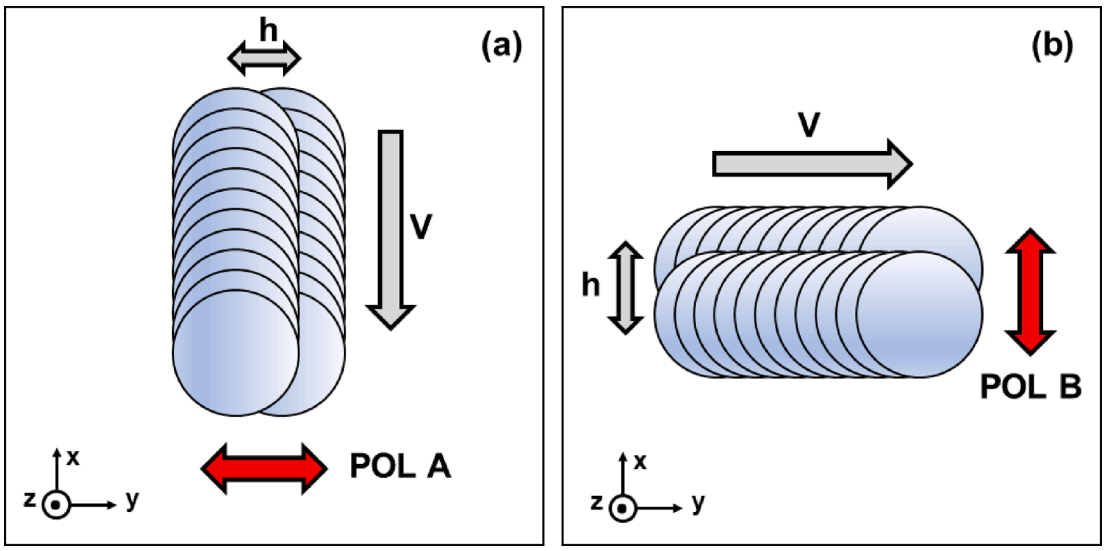

Fig. 2. Laser scanning patterns used for LIPSS texturing of quartz with POL A (a) and POL B (b). *V* is the laser beam scanning speed and *h* the hatch distance between two scanning tracks. In the bottom left corner of each panel the wafer crystalline axes orientations is shown.

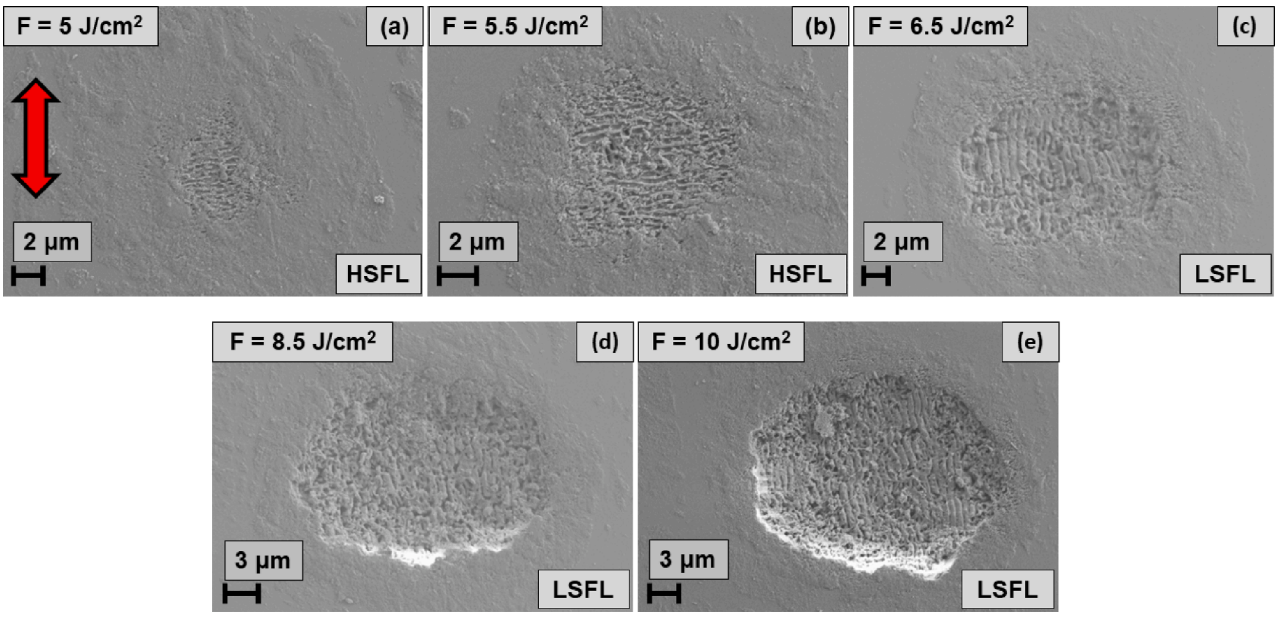

Fig. 3. SEM images of LIPSS spots on quartz surface, after irradiation with $N = 10$ linearly polarized laser pulses (red arrow in (a), referred to as POL B), at increasing laser fluences from $F = 5.0$ J/cm^2 (a) to $F = 10$ J/cm^2 (e). (For interpretation of the references to colour in this figure legend, the reader is referred to the web version of this article.)

from HSFL to LSFL, for both incident polarization directions. Within each regime, the period values were comparable, inside the uncertainty interval, for both different laser fluence *F* and polarization, so the data were averaged. The following values were obtained: $\Lambda_{HSFL} = 332 \pm 18$ nm and $\Lambda_{LSFL} = 791 \pm 29$ nm. Both these average periods are in agreement with the results found in literature for quartz [17,27].

A possible dependence of the LIPSS orientation on the crystal lattice has been also investigated. The samples employed in this work are z-cut α-quartz. α-quartz belongs to the hexagonal trigonal crystal class (also referred to as 3 2 class) which has a three-fold rotational symmetry (120°) around the c-axis of the crystal. Z-cut samples have their surfaces orthogonal to the c-axis, so their lattice is symmetric for 120° rotations. In order to investigate any influence of the crystal lattice orientation on the LIPSS orientation, additional experiments were performed producing LSFL with $F = 10$ J/cm^2 and at $N = 10$ and keeping the polarization direction fixed (POL A) while rotating the sample at steps of 30°. For every rotation angle LSFL were found to remain parallel to the polarization direction, thus it is possible to conclude that, for z-cut quartz, LIPSS orientation is not dependent on the crystal lattice orientation.

3.2. LIPSS period dependence on the number of pulses

In Fig. 5, SEM images of LIPSS spots realized at $F = 6.5$ J/cm^2, $\nu = 6$ kHz and laser pulses varying from $N = 10$ to $N = 100$ are shown.

Fig. 5(a) shows LSFL obtained, as expected, with $F = 6.5$ J/cm^2 and $N = 10$. Increasing *N* from 10 to 20 (Fig. 5(b)), the LSFL region increases in size (70 ± 1 % of total crater area) and HSFL appear around the central region. At $N = 50$, the total accumulated fluence is enough to cause ablation, and so for this reason HSFL are not formed, but LIPSS do still appear at the bottom of the ablated crater while at $N = 100$ the

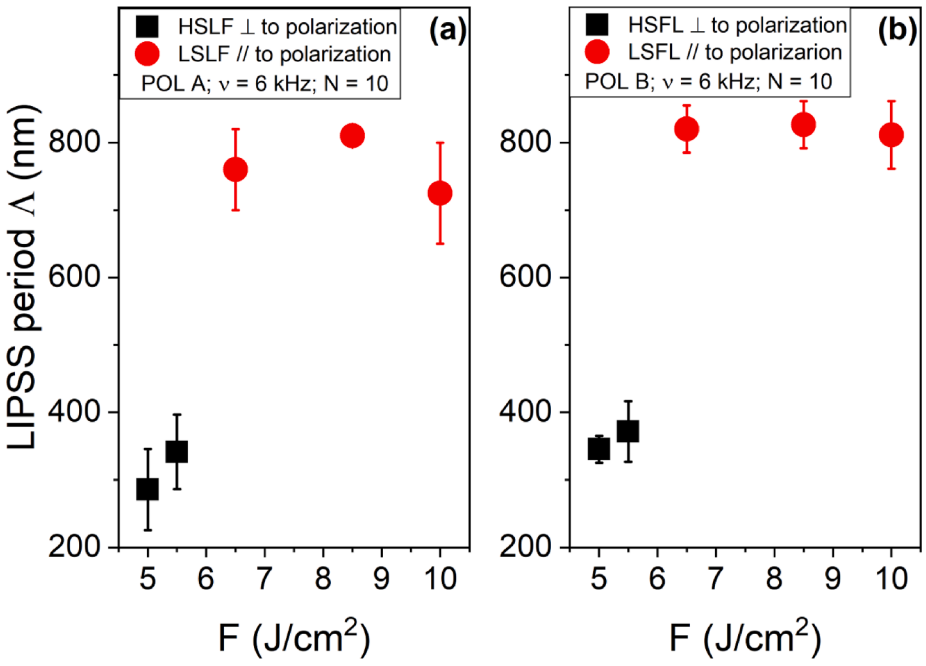

Fig. 4. LIPSS periods on quartz as function of the laser fluence F for POL A (a) and for POL B (b). Periods were measured as the average of the most frequent values deduced from the 2D-Fourier analysis of each spot and the uncertainties represent the related standard deviation ($N = 10$, $\nu = 6$ kHz).

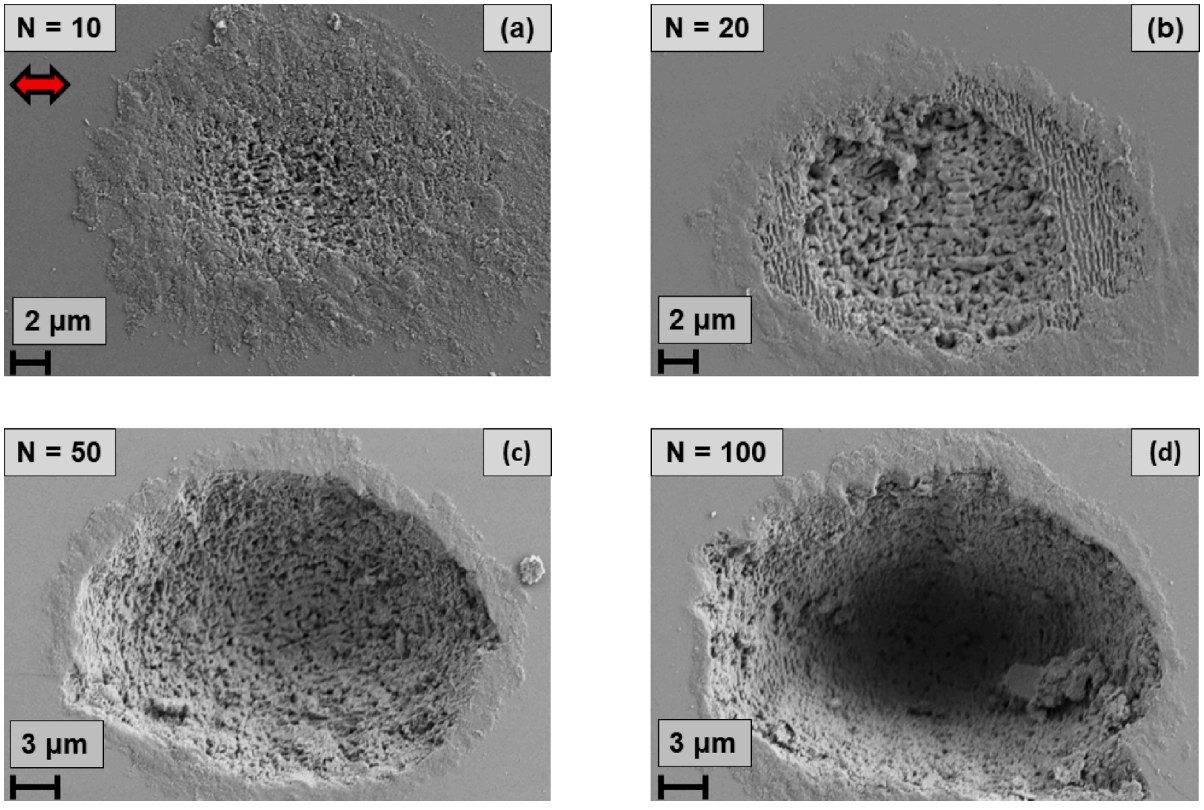

Fig. 5. SEM images of LIPSS spots on quartz surface after irradiation with $F = 6.5$ J/cm^2 at $\nu = 6$ kHz linearly polarized (POL A; red arrow in (a)) pulses going from $N = 10$ (a) to $N = 100$ (d). (For interpretation of the references to colour in this figure legend, the reader is referred to the web version of this article.)

ablated crater shows no LIPSS anymore. In Fig. 6 the LIPSS periods of the spots in Fig. 5 are plotted as a function of the number of pulses N.

HSFL manifested only at $N = 20$, with a period of 402 ± 60 nm, at the border of the crater. In this region the accumulated energy (relative to the tails of the gaussian profile of the laser beam), is sufficient only to generate HSFL, while LFSL are formed in the centre of the crater. Both HSFL and LSFL periods measured values are still comparable with those found for quartz in other works[17,27].

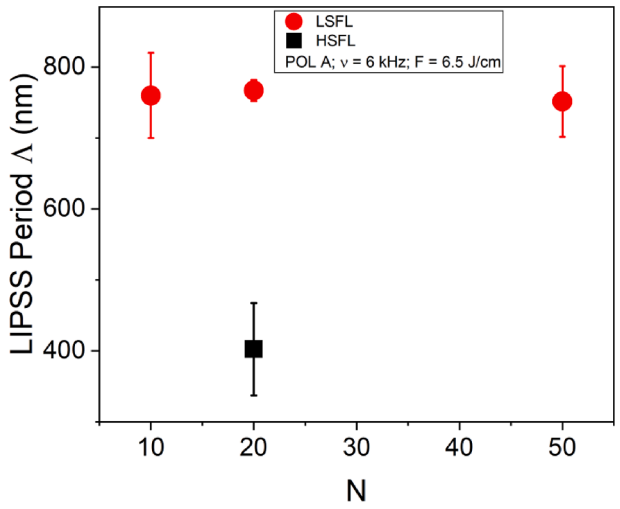

Fig. 6. – LIPSS periods in dependence on the number of pulses at F = 6.5 J/cm^2 and ν = 6 kHz.

3.3. LIPSS period dependence on repetition rate

In Fig. 7 the LIPSS periods for both LSFL and HSFL are reported as a function of the repetition rate ν, having set the number of pulses at N = 10 and the laser fluence at two different values in order to produce either HSFL or LSFL.

For the LSFL the laser fluence was fixed at $F = 8.5$ J/cm^2 while ν was varied over three values: 0.6, 6 and 60 kHz. No trend of the LSFL period Λ_{LSFL} with the repetition rate is evident. For the HSFL the laser fluence was fixed at $F = 5.5$. J/cm^2, varying the repetition rate over the same values. As for LSFL, there is no clear influence of ν on the period of the HSFL Λ_{HSFL}.

3.4. Extended LIPSS patterns on quartz for wettability applications

LIPSS patterns were realized over extended areas, up to dimension of 25 mm^2. In Fig. 8 two pictures of two such patterns are shown.

In Fig. 8(a) and 8(b) the pattern was realized by vertically scanning (horizontally in Fig. 8(b)) the selected area with lateral distance of h = 10 μm between the laser tracks, resulting in a horizontal (vertical in Fig. 8(a)) overlap of about 50 % between adjacent laser tracks. HSFL were obtained parallel to the scanning direction, being the laser polarization orthogonal to it. The periods Λ_{HSFL} measured were 440.8 ± 6.5 nm for the vertical scanned area, Fig. 9(a), and 445.2 ± 5.4 nm for the horizontal scanned area, Fig. 9(b), respectively. These two values are larger than those obtained from data in Fig. 4. This increase in period could be ascribed to an effective larger number of pulses per spot, caused by the overlap between adjacent tracks. These two areas were used to investigate the effect of LIPSS on quartz wettability.

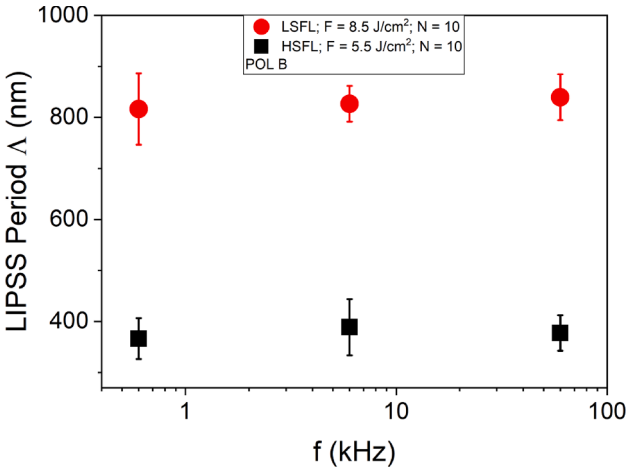

Fig. 7. LIPSS periods in dependence on the repetition rate for two different values of fluence (N = 10).

Pristine quartz is a hydrophilic material; in Fig. 9 the image of a 3 μL water droplet deposited on a non-textured quartz sample is shown.

The contact angle CA, evaluated over four droplets, was found equal to $\theta_{av} = 41.2 \pm 0.3°$, confirming the quartz hydrophilic behaviour. In Fig. 10 the image of a droplet of 3 μL on LIPSS textured areas is shown.

The CA is found to be equal to 7.6° which is below 10°, which is the threshold CA value between hydrophilic and super hydrophilic behaviour [28]. The change in the material wetting behaviour was attributed to change in surface topography (LIPSS) which suggests that Wenzel state of wetting. Any chemical modification influence on the wetting behaviour is considered negligible since samples were textured in ambient air and that quartz is very chemically stable[29].

These two scanning strategies were chosen in order to evaluate any influence of the crystalline orientation on the LIPSS generation. As stated before, since both HSFL periods and the wettability results are ultimately comparable for the two scanning strategies, it is safe to assume no influence crystalline orientation on the LIPSS formation.

Superficial resistivity measurements [30] were performed in order to evaluate possible sensing applications of these super-hydrophilic LIPSS patterns. These measurements were performed using a quartz wafer having two test areas both of 25 mm^2: the first consisted in a continuous LIPSS pattern and second was pristine quartz. The sample was kept in the chamber up until the vapour concentration inside reached the saturation value. The sample was then taken out from the chamber and a resistivity measurement was carried out using the probes of a digital multimeter placed at opposite angles of the LIPSS patterned area and of the untextured area. Being quartz an insulant material, the multimeter would measure the resistivity through the water deposited on the sample surface. An infinite resistance value was measured on the untextured area: this is probably due to the fact that on the pristine quartz water is deposited in the form of non-adjacent droplets. The textured area, instead, showed a resistivity value of 5.5 ± 0.1 MΩ, suggesting that the enhancement of hydrophilicity of textured quartzfacilitates the deposition of water on the target surface. The texturing approach is potentially cheaper and faster since it does not require any chemical treatment or any addition of complex films to the sensing quartz element[25].

4. Conclusion

In this work, we investigated the parameter space of LIPSS generation on quartz crystal surfaces. The LIPSS formation was evaluated as a function of the laser fluence F, the number of laser pulses N and laser pulse repetition rate ν. The LIPSS orientation was always found parallel to polarization for LSFL and perpendicular for HSFL. This remained true whatever the polarization direction, thus excluding any influence on the crystal structure on LIPSS orientation. The average values of LSFL and HSFL periods were found to be in good agreement with the results found in literature for quartz. It was also determined that the periods are not influenced by the repetition rate.

Finally extended LIPSS patterns, in HSFL regime, were realized over areas of 25 mm^2 and were found to greatly enhance the hydrophilicity of quartz. This was verified through contact angle measurements, which show a decrease of the average contact angle from 41.2° to 7.6°, indicating a transition from hydrophilicity to super-hydrophilicity of the quartz surface. This result opens the way to the application of to quartz crystals for humidity sensing, possibly improving and simplifying the design of such devices, which as of today employ QCM integrated with active layers upon quartz substrates [25].

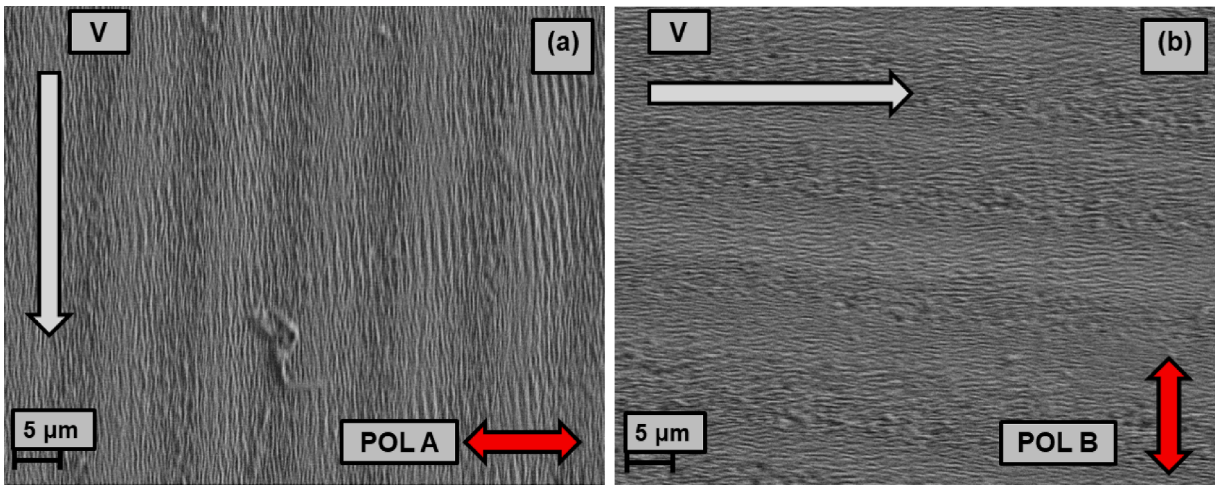

Fig. 8. HSFL patterns realized at the polarizations, POL A (a) and POL B (b), (red arrows) and each perpendicular to the scan direction (grey arrows). (For interpretation of the references to colour in this figure legend, the reader is referred to the web version of this article.)

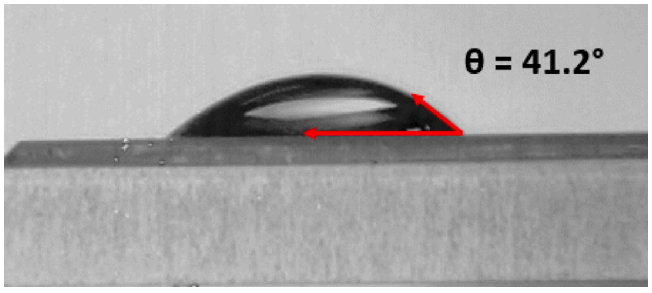

Fig. 9. Contact angle measure for a 3 μL water droplet on non-textured quartz.

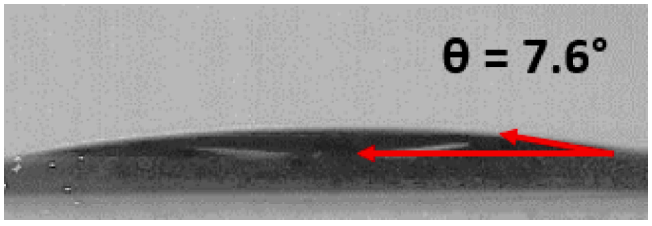

Fig. 10. Contact angle measure for a 3 μL water droplet on LIPSS-textured areas.

CRediT authorship contribution statement

Raffaele De Palo: Conceptualization, Investigation, Formal analysis, Visualization, Writing – original draft. **Antonio Emanuele Mazzarone:** Investigation, Formal analysis, Visualization, Writing – original draft. **Annalisa Volpe:** Conceptualization, Formal analysis, Visualization, Writing – review & editing, Supervision. **Caterina Gaudiuso:** Writing – review & editing. **Francesco Paolo Mezzapesa:** Writing – review & editing. **Vincenzo Spagnolo:** . **Antonio Ancona:** Formal analysis, Writing – review & editing.

Declaration of Competing Interest

The authors declare that they have no known competing financial interests or personal relationships that could have appeared to influence the work reported in this paper.

Data availability

Data will be made available on request.

References

[1] Y. Saigusa, Quartz-Based piezoelectric materials, Adv. Piezoelectric Mater. 197–233 (2017).
[2] P. Patimisco, A. Sampaolo, H. Zheng, L. Dong, F.K. Tittel, V. Spagnolo, Quartz-enhanced photoacoustic spectrophones exploiting custom tuning forks: a review, Adv. Phys. 2 (1) (2017) 169–187.
[3] R.E. Speight, M.A. Cooper, A survey of the 2010 quartz crystal microbalance literature, J. Mol. Recognit. 25 (9) (2012) 451–473.
[4] A. Sampaolo, P. Patimisco, M. Giglio, A. Zifarelli, H. Wu, L. Dong, and V. Spagnolo, "Quartz-enhanced photoacoustic spectroscopy for multi-gas detection: A review," (2021).
[5] T. Wei, A. Zifarelli, S. Dello Russo, H. Wu, G. Menduni, P. Patimisco, A. Sampaolo, V. Spagnolo, L. Dong, High and flat spectral responsivity of quartz tuning fork used as infrared photodetector in tunable diode laser spectroscopy, Appl. Phys. Rev. 8 (4) (2021).
[6] A. Zifarelli, A. Sampaolo, P. Patimisco, M. Giglio, M. Gonzalez, H. Wu, L. Dong, V. Spagnolo, Methane and ethane detection from natural gas level down to trace concentrations using a compact mid-IR sensor based on light-induced thermoelastic spectroscopy and univariate calibration, Photoacoustics 29 (2023), 100448.
[7] D.A. Buttry, Applications of the quartz crystal microbalance to electrochemistry, Electroanal. Chem. 1–85 (2021).
[8] A.Y. Vorobyev, C. Guo, Direct creation of black silicon using femtosecond laser pulses, Appl. Surf. Sci. 257 (16) (2011) 7291–7294.
[9] P. Calvani, A. Bellucci, M. Girolami, S. Orlando, V. Valentini, R. Polini, D. M. Trucchi, Black diamond for solar energy conversion, Carbon N. Y. 105 (2016) 401–407.
[10] A. Volpe, S. Covella, C. Gaudiuso, A. Ancona, Improving the laser texture strategy to get superhydrophobic aluminum alloy surfaces, Coatings 11 (3) (2021).
[11] A. Volpe, C. Gaudiuso, L. Di Venere, F. Licciulli, F. Giordano, A. Ancona, Direct femtosecond laser fabrication of superhydrophobic aluminum alloy surfaces with anti-icing properties, Coatings 10 (6) (2020).
[12] A. Volpe, C. Gaudiuso, and A. Ancona, "materials Laser Fabrication of Anti-Icing Surfaces: A Review," (n.d.).
[13] F. Piscitelli, R. De Palo, A. Volpe, Enhancing coating adhesion on Fibre-Reinforced composite by femtosecond laser texturing, Coatings 13 (5) (2023).
[14] J. Bonse, S. Höhm, S. V Kirner, A. Rosenfeld, and J. Krüger, "Laser-Induced Periodic Surface Structures-A Scientific Evergreen," IEEE J. Sel. Top. QUANTUM Electron. **23**(3), (n.d.).
[15] A. Borowiec, H.K. Haugen, Subwavelength ripple formation on the surfaces of compound semiconductors irradiated with femtosecond laser pulses, Appl. Phys. Lett. 82 (25) (2003) 4462.
[16] A.Y. Vorobyev, V.S. Makin, C. Guo, Periodic ordering of random surface nanostructures induced by femtosecond laser pulses on metals, J. Appl. Phys. 101 (3) (2007), 034903.
[17] S. Höhm, A. Rosenfeld, J. Krüger, J. Bonse, Femtosecond laser-induced periodic surface structures on silica, J. Appl. Phys. 112 (1) (2012).
[18] D. Dufft, A. Rosenfeld, S.K. Das, R. Grunwald, J. Bonse, Femtosecond laser-induced periodic surface structures revisited: A comparative study on ZnO, J. Appl. Phys. 105 (3) (2009), 034908.
[19] T.Q. Jia, H.X. Chen, M. Huang, F.L. Zhao, J.R. Qiu, R.X. Li, Z.Z. Xu, X.K. He, J. Zhang, H. Kuroda, Formation of nanogratings on the surface of a ZnSe crystal

irradiated by femtosecond laser pulses, Phys. Rev. B - Condens. Matter Mater. Phys. 72 (12) (2005), 125429.
[20] M. Soldera, F. Fortuna, S. Teutoburg-Weiss, S. Milles, K. Taretto, A.F. Lasag, Comparison of structural colors achieved by laser-induced periodic surface structures and direct laser interference patterning, J. Laser Micro Nanoeng. 15 (2) (2020).
[21] G. Giannuzzi, C. Gaudiuso, R. Di Mundo, L. Mirenghi, F. Fraggelakis, R. Kling, P. M. Lugarà, A. Ancona, Short and long term surface chemistry and wetting behaviour of stainless steel with 1D and 2D periodic structures induced by bursts of femtosecond laser pulses, Appl. Surf. Sci. 494 (2019).
[22] J. Bonse, R. Koter, M. Hartelt, D. Spaltmann, S. Pentzien, S. Höhm, A. Rosenfeld, J. Krüger, Femtosecond laser-induced periodic surface structures on steel and titanium alloy for tribological applications, Appl. Phys. A Mater. Sci. Process. 117 (1) (2014) 103–110.
[23] O. Raimbault, S. Benayoun, K. Anselme, C. Mauclair, T. Bourgade, A.M. Kietzig, P. L. Girard-Lauriault, S. Valette, C. Donnet, The effects of femtosecond laser-textured Ti-6Al-4V on wettability and cell response, Mater. Sci. Eng. C 69 (2016).
[24] M. Girolami, A. Bellucci, M. Mastellone, S. Orlando, V. Serpente, V. Valentini, R. Polini, E. Sani, T. De Caro, and D. M. Trucchi, "materials Femtosecond-Laser Nanostructuring of Black Diamond Films under Different Gas Environments," (n. d.).
[25] A. Rianjanu, T. Julian, S.N. Hidayat, N. Yulianto, N. Majid, I. Syamsu, H.S. Wasisto, K. Triyana, Quartz crystal microbalance humidity sensors integrated with hydrophilic polyethyleneimine-grafted polyacrylonitrile nanofibers, Sensors Actuators B Chem. 319 (2020), 128286.
[26] R. De Palo, A. Volpe, C. Gaudiuso, P. Patimisco, V. Spagnolo, A. Ancona, Threshold fluence and incubation during multi-pulse ultrafast laser ablation of quartz, Opt. Express 30 (25) (2022) 44908–44917.
[27] J. Bonse, J. Krüger, S. Höhm, A. Rosenfeld, Femtosecond laser-induced periodic surface structures, J. Laser Appl. 24 (4) (2012), 042006.
[28] A. Samanta, Q. Wang, S.K. Shaw, H. Ding, Roles of chemistry modification for laser textured metal alloys to achieve extreme surface wetting behaviors, Mater. Des. 192 (2020), 108744.
[29] A. Ouchene, G. Mollon, M. Ollivier, X. Sedao, A. Pascale-Hamri, G. Dumazer, E. Serris, Roughness and wettability control of soda-lime silica glass surfaces by femtosecond laser texturing and curing environments, Appl. Surf. Sci. 630 (2023).
[30] Y. Seki, A. Altinisik Tagac, surface resistivity, surface wettability and thermal stability of the 1-ethyl-2,3-dimethylimidazolium ethyl sulfate and methyl-tri-n-butylammonium methyl sulfate modified polyethylene, Polym. Technol. Mater. 59 (7) (2020).